Neutron radiography for visualization of liquid metal processes: bubbly flow for CO_2 free production of Hydrogen and solidification processes in EM field

You may also be interested in:

Neutron radiography for visualization of liquid metal processes: bubbly flow for CO$_2$ free production of Hydrogen and solidification processes in EM field

E Baake[1,*]**, T Fehling**[1]**, D Musaeva**[1,2] **and T Steinberg**[1]

[1]Institute of Electrotechnology, Leibniz University of Hannover, Wilhelm-Busch Str. 4, DE 30167 Hannover, Germany
[2]Kazan State Power Engineering University, Krasnoselskaya Str. 51, RU 420066 Kazan, Russian Federation
*baake@etp.uni-hannover.de

Abstract. The paper describes the results of two experimental investigations aimed to extend the abilities of a neutron radiography to visualize two-phase processes in the electromagnetically (EM) driven melt flow. In the first experiment the Argon bubbly flow in the molten Gallium – a simulation of the CO$_2$ free production of Hydrogen process – was investigated and visualized. Abilities of EM stirring for control on the bubbles residence time in the melt were tested. The second experiment was directed to visualization of a solidification front formation under the influence of EM field. On the basis of the neutron shadow pictures the form of growing ingot, influenced by turbulent flows, was considered. In the both cases rotating permanent magnets were agitating the melt flow. The experimental results have shown that the neutron radiography can be successfully employed for obtaining the visual information about the described processes.

1. Introduction

Liquid metals are used in various industrial applications and processes. One new approach to produce hydrogen without CO$_2$ emission is the thermal cracking of methane. To deliver the high temperature ambience for methane cracking, liquid tin is used at temperatures above 660 °C. In order to study multi-phase phenomena in the reactor, a method is demanded, that is able to penetrate even heavy metal atoms to visualize gas bubbles in opaque media.

Another process, where visualization of physical phenomena in opaque liquid metal is demanded, is an influence of electromagnetic stirring on a solidification processes. Electromagnetic (EM) stirring of a solidifying melt is a well-known approach in industry to enhance material quality. However, physical effects like development of vortices in the liquid part of the melt and the effect on the development of the solidification front can be studied very carefully using a technology, that is able to visualize these effects.

In the history of liquid metal research many methods have been investigated to characterize effects in the melt. Outstanding investigations have been performed by Tarapore and Evans in 1977 [1], who investigated non-invasively the velocity distribution of stirring effects by using strobosophic photography of the free surface of liquid metal. Later Moore and Hunt (1983) [2] used invasive methods like drag probes and hot film anemometer to estimate velocities inside the liquid metal. The approach from non-invasive to invasive methods shows the big problem to visualize physical effects in opaque liquid melt. Later Umbrashko (2006) [3] and Kirpo (2007) [4] investigated turbulence

fluctuations in induction crucible furnaces (ICF) using potential probes and numerical simulation tools. Till now the most common method, which could be implemented for obtaining visual information about the two-phase flows was X-ray attenuation [5-7]. Applicability of this method is limited by the thickness of the melt volume under investigation. In this kind of systems, a development of turbulence is limited as well.

One of the solutions in this area was an application of the well-developed methods of the neutron radiography. Here the samples thickness limited as well by the neutron flux and attenuation of the material, but not in such a critical way, so the turbulent phenomenon can find a place. The first experiments on this field were performed three decades ago by American scientific group from Minneapolis. Such a processes as diffusion and dispersion in porous media [8] were investigated by means of neutron radiography and have showed its potentialities. The solidification process of the metal and segregation processes were visualized as well with beam of thermal neutrons [9]. Newly, Wondrak et. al (2014) [10] developed the non-invasive Contactless Inductive Flow Tomography (CIFT) using tomography and numerical simulation to visualize velocity distribution inside liquid metal. In this time Saito et al. [11] started to investigate liquid metal flow and especially the formation of gas bubbles in liquid metal using neutron radiography. In this experiment gas bubbles from vaporized water in Pb-Bi eutectic has been detected. This experiments and first successful experiments of Sarma et al. in 2015 [12], aimed to visualize particle admixture in liquid metal gave the idea to try to use neutron radiography for studying gas bubble dynamics in liquid metal and EM influenced solidification processes more carefully.

Whereas the neutron radiography technology improves during all this time, there are no systematic investigations of liquid metal bubbly flows and solidification processes by Neutron radiography so far. In general, many previous experimental studies exist carried out using other diagnostic techniques. The goal of this research is to test the abilities of the neutron radiography for visualization the two-phase process. This paper contains on the one hand experiments on visualizing gas bubble dynamics in liquid metal and on the other hand solidification of metal under the influence of externally applied EM fields.

2. Motivation

2.1. Visualization of a bubbly flow in a melt for CO_2 free production of Hydrogen

For production of ecologically friendly hydrogen compared to common steam reforming process, the thermal cracking of methane can be considered as an alternative route. The thermal cracking takes place in a high temperature environment. At temperatures above 600°C methane (CH_4) decomposes to $C + 2H_2$ (Δh_0=74,85 kJ/mol). To explore the potential of carbon dioxid free production via thermal decomposition of methane, experiments were realized by a small scale experimental bubble column reactor. Here methane bubbles are inserted via an orifice and rise up in a column filled with liquid tin at temperatures higher than 600°C. One problem in this setup is the missing possibility of viewing the dynamics inside the reactor. Especially the optimization of the bubbles residence offers the chance to increase the hydrogen yield. Based on that fact, numerical simulations (figure 1, a-d) have been done to show the dynamics and to calculate possible improvements. The numerical modelling includes studies for different initial bubble sizes, volume flows, inlet types and geometry as well as feasibilities of electromagnetic stirring. A detailed description of the studies can be found in [13]. To get a numerical result of the bubble dynamics models for the physics of the two-phase flow have to be used. In the discovered cases an Euler-Euler-description is used based on an initial observer formulation of the two phases. Based on this formulation an Eulerian method [14] is used with regards to a more exact calculation for greater bubble volume fractions and greater Stokes numbers, especially at the surface and for different velocities of the phases. In this method a separated set of equations is solved for every phase. Parameters for phase exchange to describe the gas liquid interface (Schiller-Naumann) as well as heat transfer coefficients (Ranz Marshall) can be specified by correlations.
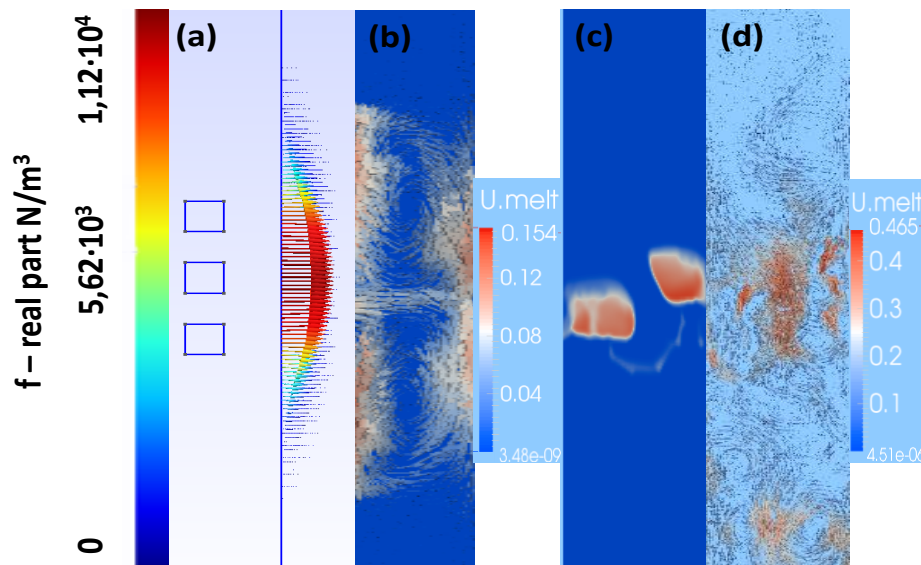
Figure 1. Numerical simulation results: Lorentz force for an AC EM-field in left half (a) and resulting velocity [m/s] in right half (b) of the column, split for a 20 mm bubble (c) and velocity field around the split bubble (d) for whole column diameter.

To get an idea about the residence times of different single bubble sizes in the reactor different residence times for initial bubble diameters have been discovered in the numerical simulation. It can be seen that bubble residence times decrease with bubble diameter down to a minimum until the occurrence of oscillations that decrease the velocities. Further increasing the diameter leads to bubble shape changes which decreases the residence time again. These effects can occur for different gas-liquid flows. In actual studies also the effect of an electromagnetic field on the bubbles dynamics has been discovered [23]. It has been shown that a bubbles breakup and as a result an increase of residence time can be achieved. This has been done for different initial bubble sizes to discover possibilities for breakup as a function on bubble diameter. Figure 1 shows the dynamics under influence of an AC electromagnetic field generated by a coil in the middle of the reactor. The resulting Lorentz forces generate whirl structures in the melt. Afterwards a single bubble is introduced into the reactor. Depending on frequency and current a split into blebs can be achieved due to turbulent shear forces. Numerical simulations investigated breakup possibilities and influence on residence time for different bubble diameters. Another potential is given the usage of packed and multi-inlets, that has also been simulated. It has to be mentioned, that also wall effects also reduced the averaged magnitude of bubble velocities. Due to this and the effect of carbon sediments at the reactor surface, also greater bubbles near the reactor diameter have been discovered. This also leads to the question which bubble sizes are generated in continuous volume flows and how they behave in bubble collectives. Simulations show the effect of wobbling appearance when increasing the volume flow. To get a view on the effects of volume flows experiments with neutron radiography have been done.

2.2. Visualization of a formation of a solidification front
The structures which form during the solidification of a material play an enormous role in the properties of the solid material. It is well known, that application of EM stirring to the solidifying material can provide more homogeneous and fine structure, which is more desirable in the metallurgy. Due to intensive turbulent flows an efficient EM stirring leads to an absence of high temperature gradients in the melt, pinning of growing grains due to the melt motion, partial re-melting of the structure under formation [15, 16]. At the same time, a development of such undesired effects as a macro-segregation as well can be a consequence of the intensive melt motion [17] Consequently, an optimization of application of EM stirring to the crystallizing metal is required. Different magnetic

fields, such as rotating, travelling, pulsating, and their different combinations, are available for the optimization of stirring process and for creating the flow patterns in the melt, adjusted according to the requirements. One of optimized stirring methods is an application of EM field with pulses. In such a conditions intensive stirring periods are interleaved with pause periods, when the segregation effects could be reduced. Bright illustration of an effect of pulsed EM stirring was obtained in the numerical and experimental investigations and described by S. Eckert et. al (2007) [18], B. Willers et. al (2008) [19] and X. Wang et. al (2009) [20]. These scientific groups observed an influence of an application of travelling and rotating magnetic fields modulated at low-frequency pulses to solidifying metal. It was shown, that an optimized forcing of the melt can lead to more homogeneous and fine metal structure. Nevertheless, up to now it is an open question – how the turbulent electromagnetically driven flows interact with a solid phase? The knowledge about a process, happening in the solidifying material is a key for improving existing technologies of high quality materials production and should have to be extended by means of new investigation techniques.

Due to the liquid metals opaqueness an obtaining of spatial information about a solidification process is one of the challenging problems. Up to now the most common method, which could be implemented for obtaining visual information about the interaction of solid and liquid phases during an EM stirring was X-ray attenuation. But a limitation of a thickness of the systems for X-ray analysis does not give ability to analyse its influence of 3 dimensional turbulent flows on an ingot formation, although particularly intensive turbulent flows and flow structures with high wave number have the strongest influence on the growing crystals [16]. So the search and improvement of visualization techniques for metallurgy is one of the current scientific tasks. A principle of neutron radiography seems to be feasible for obtaining an information about a solidification process development through time and observing the influence of EM stirring. So the technique was applied to visualize and analyse a change of a solidification front form, as a consequence of an intensive EM stirring.

3. Neutron radiography

Nowadays the method of neutron radiography develops rapidly and extends the ranges of physical phenomena which can be analysed with its application. The principal on which it is based can be described as following: in the real-time image system for visualisation of dynamic processes the 2D distribution of the transmitted neutron beam intensity through a sample is measured. The illuminating neutron beam, controlled to be almost parallel, meets on its way the sample and the neutron flux, passing through the material decreases. Then on the back side of the sample the neutron beam with decreased flux passes through the scintillator which converts neutrons to the light emission. The light output could be processed with the imaging detectors covering the illuminated sample area. In most cases this is a digital camera system looking onto a thin neutron scintillator screen. The recorded stack of digital pictures can be converted into a video sequence. The required exposure time determines the frame rate.

The most important requirement here is an attenuation coefficient of analysed sample which should have to be adjusted so to provide a high contrast in the transmission image. For that can be suitable very few materials, such as Gadolinium, Cadmium, and Boron. Materials with low attenuation coefficient are virtually transparent to the thermal neutrons. Although the combination of materials with different attenuation coefficients could be used as well for imaging of some processes, such as flow tracers in porous media [8]. When applying the neutron radiography to the pure materials one can use the dependence of the thermal neutron flux on the density of the material, so such processes as solidification or melting of the materials with initially high enough attenuation coefficient can be visualized. According to the equation (1) the neutrons transmission through the melt volume depend on the density ρ, the thickness x of the sample, neutron flux I and could be expressed by exponential relation between these parameters [21]:

$$\frac{I}{I_0} = \exp\left(-\mu\rho x\right) \tag{1}$$

where μ [cm^2/g]– is the thermal neutron cross-section of the object, I_0 [neutrons·cm^{-2}·sec^{-1}·mA^{-1}] – incident thermal neutron flux. In case of use of different materials, as well as solid and liquid phases of the solidifying material, a difference in a density and, consequently, difference in the attenuation, provides the neutron shadow images.

In comparison to X-ray, neutron radiography has contrary characteristics in relation to attenuation coefficient. Whereas, X-rays interact mainly with the electrons of an atom and thus have low penetration depths for heavy materials like metals, neutrons interact with atomic core directly and shows high attenuation for atoms like Hydrogen, Boron, Cadmium, etc.

Saito et. al [11] used neutron radiography and Particle Image Velocimetry (PIV) techniques to study the effect of recirculation flow on the bubble behaviour. The dynamics of molten lead bismuth as liquid metal and nitrogen as gas bubbles in a rectangular tank were studied. Additionally, particles made of gold-cadmium (AuCd$_3$) inter-metallic alloy were used as tracers for calculation of flow field using PIV. From these results basic characteristics of liquid-metal and gas dynamics have been clarified. Sarma et al. [12] used neutron radiography and PIV method to study the motion of particles in the liquid metal, which was stirred by a magnetic field applied from four counter rotating permanent magnets. Carried out results show that neutron radiography is a suitable method for investigations of multi-phase flow. Animated from these results the application of neutron radiography to visualize liquid-gas multi-phase flows and solidification processes seems very promising.

In this paper two experiments directed on visualization of two-phase process (gas bubbles flow in the melt and a solidification) by means of pure Gallium, forced by an alternating electromagnetic field, is described and discussed. Abilities of a thermal neutron beam were tested to provide information about the influence of the melt flows on the processes.

4. Experimental setups and procedures

Experimental setup (figure 2) was designed to provide 2D snapshots of the processes, happening in the melt bath. For that the vessel, containing the liquid Ga, was made in a rectangular form to be placed before the beam of neutrons. The construction of the experimental unit was inspired by those, used by the scientific group and described in [12]. Liquid metal flows were agitated by the stirrer on rotating permanent magnets. Material properties of Gallium and magnets are presented in the table 1. According to the aim of the experiment a construction of the setup differed and described below for the both cases.

Table 1. Properties of materials, used in the experiment.

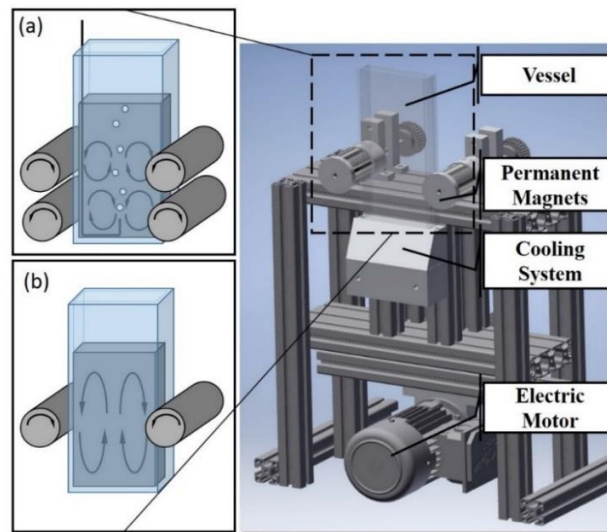| Variable	Symbol	Value
Gallium		
Melting temperature, ℃	t_{melt}	29,8
Weight, kg	m	1,4
Electric conductivity, S/m`	σ	$3{,}7\cdot10^6$
Density, kg/m^3	$\rho,$	
	at $t > t_{melt}$	6080
	at $t < t_{melt}$	5910
Attenuation coefficient for thermal neutrons, cm^{-3}	K	0,49
NdFeB Magnets		
Remanence on the surface, T	Br	1,17
Coercivety, A/m	Hc	$13{,}5\cdot10^5$

Figure 2. Sketch of the experimental setup and the direction of magnets rotation and flows in the liquid Ga: (a) – gas bubbly flow experiment; (b) – solidification experiment.

4.1. Bubbly motion under the influence of EM driven melt flow

The vessel with the size of 300 mm x 140 mm x 25 mm (figure 2, a) was made of PEEK material to avoid chemical reactions with the frame of the vessel. Gallium has been chosen for liquid metal, because of its low melting point and working safety. Specially designed particles with a lead kernel and glued boron carbide, fitting to attenuation coefficient and density to fulfil admixture ability, were used as particles and tracers for PIV simultaneously. Instead of methane Argon gas has been used, due to its easy availability in industrial processes and in laboratories like Swiss Spallation Neutron Source (SINQ) at Paul Scherrer Institute, Villigen, Switzerland. The attenuation coefficient for Ga is with 0,49 appr. 16 times higher compared to coefficient of Ar (0,03). Since the neutron beam is attenuated much more by Ga and less by Ar, Ar bubbles appear as bride spots on the camera (figure 3, a). For gas inlet capillary tubes made of stainless steel with an outer diameter of 1.5 mm and inner diameter between 0.5 – 1.3 mm connected to an automated gas controller have been used. The formation of bubbles has been studied by differently sized inlet diameters of capillary tubes, as well as their velocity and trajectory in the reactor. Furthermore, impact on bubbly flow by applied electromagnetic field by two and four counter-rotating magnets has been studied.
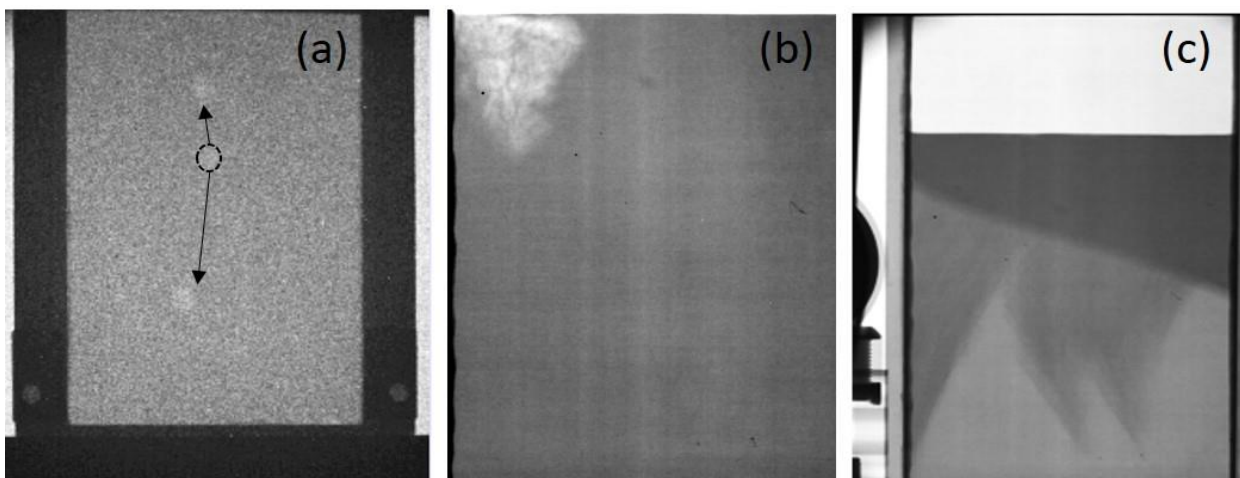

Figure 3. Raw neutron images: (a) – gas bubbly flow experiment; (b) – crystals of Ga on the free surface of the melt, appeared due to the cooling of the camera; (c) – Ga solidification experiment.

In the experiment, four counter rotating magnets have been used to create a mixing inside of the melt. The rotation of permanent magnets creates four vortices in a plane. The structure has been chosen that the velocity in the middle of the vessel is opposed to the ascending motion of the bubbles. This experimental setup has been used from Sarma, Scepanskis et. Al. [12] for investigation of the distribution of particles inside of liquid metal flow. Due to a joint experimental stay at PSI this setup has been used and further developed for bubbly flow and solidification experiments. Two effects should be investigated: 1) Breakup of bubbles due to shear stress induced by the rotation of the magnets, 2) impact on the size of the bubbles, their velocity and thus their residence time.

The camera, used to obtain the neutron shadow images, was intensively cooled during the experiment. The cooled air, reaching the free surface of the liquid Ga provided the conditions of its solidification. Although it was an undesired effect according to the aims of the gas bubbly flow investigation, the both solid and liquid phases of Ga were recognized on the obtained pictures (figure 3, b). This became a seed for the idea and a preliminary experiment for the investigation of solidification front formation described below.

4.2. Gallium solidification experiment
The experimental setup (figure 2, b) was used to obtain 2D snapshots of the Ga solidification front formation influenced by an electromagnetic field. For the material of the vessel a window glass (SiO_2 $^{72\%}$ $Na_2O^{14,2\%}$ $CaO^{10\%}$ $MgO^{2,5\%}$ $Al_2O_3^{0,6\%}$) was chosen, due to its transparency for the beam of thermal neutrons [21]. Inner dimensions of the vessel were H x L x W: 20 x 10 x 2 cm. A weight of Ga, placed in the vessel, was 1,4 kg (corresponds to 12 cm height of the melt). The vessel with Ga was preliminary pre-heated and held with the temperature of 40℃. The vessel was fixed on the cooling system, providing a temperature of 12℃ during the experiment to realize a temperature gradient for directional solidification of the metal (2,3 K/cm).

The formation of solidification front and its movement was observed for three different types of conditions: solidification of the melt in constant magnetic field (DC), a convection, forced by AMF and a melt flow, driven by AMF applied with pulses.

As in the prototype setup magnetic fields were applied with use of NdFeB permanent magnets, placed beside the vessel as it shown on the figure 2, b. The magnets sets had a cylindrical form (diameter / length – 60 / 90 mm) and consisted of two pairs of magnets of different polarization. An electric motor was used to bring the magnet sets to rotation. Movement of the magnets sets was providing an appearance of AMF and Lorentz force in the metal, what was bringing the melt to the motion. The alternating frequency of magnetic field was equalled to the frequency of changing of the magnets poles with the angular frequency of rotation f_{ac} = 23,3 Hz. The disposition of magnets made possible to realize the melt flow during solidification without placing anything except the metal on the way of the neutron beam. Distance between the side of the magnet and the melt was 7 mm.

An application of PMF was realized by switching the electric motor on and off with predetermined frequency $f_p = 1 / (T_{act} + T_0)$, where T_{act} – is the period of stirring and T_0 – is the period, when the magnets do not rotate. Influence of a PMF with four values of f_p = 0,025; 0,05; 0,1 and 0,25 was analysed. For all values of f_p the duration of both periods was equal $T_{act} = T_0$. A development of a form of solidification fronts through the experiment time and a density of the grown ingots was compared for all cases.

The figure 2, b demonstrates the stream-lines of the melt flow, formed under the influence of the magnets rotation. Such a melt flow is a reproduction of the liquid metal circulation forced by application of a travelling magnetic field in an ingot-forming equipment [22].

Material's solid and liquid phases having a difference in a density and, consequently, difference in ability for neutrons attenuation, provided the neutron shadow images. Figure 3, c demonstrates the initial raw image, where with darker grey the melt and with lighter colour – the solid part of the metal can be recognized. As well partially can be seen the magnets, which are demonstrating a high contrast due to the high neutrons attenuation.

5. Experimental results and discussions

5.1. Bubbly flow in the melt

The neutron beam carries information about the material inside of the vessel. Since the attenuation coefficient of Argon is less than the attenuation coefficient of Gallium, the beam is more intense in areas of the gas bubbles. The pictures with the information are available as raw images. For post-processing the free software ImageJ has been used. Standard filters for image processing are available as part of the library of the software. The part of the picture containing the melt and the gas bubbles has been cropped. In order to highlight the gas bubbles a bandpass filter has been applied, following by an edge detection algorithm. The edge detection has been applied two times to highlight the shape of the bubbles. This procedure has been done for the whole video sequence. Thus, the development of bubbles ascending from capillary tubes, as well as their velocity can be detected (figure 3, a). Figure 3 a) gives a scale of the bubble size according to the vessel, which is 140 mm in width. Bubbles shown in the picture have in this case a size of around 6 mm.

Figure 4 shows the bubble rise velocity in dependency of Ar volume flow rate. The capillary tube has an outer diameter of 1,5 mm and an inner diameter of 0,1 mm. Velocities are calculated from bubble formation at the capillary tube to frame of the picture. In order to follow the trajectory, the middle point of each bubble in the image has been calculated and followed from previous to next picture linearly. Velocities presented are the average value of a bubble ascending from bottom to top. In the experiments bubbles ascended in a bubble chain of $3 - 5$ for gas volume flow rates below 100 sccm. At flow rates of above 100 sccm continuous chains started to appear. All in all, bubbles ascend in a zig-zag movement. The CCD camera used for the experiments was used with the following acquisition parameters: frame rate of 35.7 fps, an exposure time of 0.028 s and a pixel binning of 4x4. Since bubble formation is a very sensitive process depending on gas flow, pressure from liquid metal on the inlet, which is related to flow situation in the vessel and depends on the previous bubble flow, angle of capillary tube etc. velocity of ten bubble formation has been evaluated and averaged. In figure 4, the velocity including error bars, which represents the maximum and minimum bubble velocity of each flow rate are shown. Although, the bubble velocities are highly fluctuating, at the average of appr. 23%, a tendency of increasing velocity by increasing volume flow can be detected.

The bubble size formation for increasing volume flow rate is likewise highly fluctuating. The detected tendency by increasing volume flow rate is a decrease in bubble diameter. A smaller bubble size is proportional to reduced Archimedes force, which is the driving force for the velocity. Thus, with a smaller bubble size, the tendency of bubble velocity should also be decreasing. Bubble velocity is also influenced by previous bubbles. The conditions in the wake of a bubble and the flow situation in the vessel may lead also to a faster bubble rise and an increase in bubble velocity. Applying induced forces by rotation of permanent magnets, shows a stabilization of rising velocity independent of bubble size distribution at appr. 20,5 cm/s (figures 6 and 7). The bubble formation is still highly oscillating, although the bubble size distribution compared to bubble formation at the same flow rate of 100 sccm (Standard Cubic Centimeters per Minute) without applied magnetic field appears in average much smaller. In this case the liquid metal flow is directed to the inlet and changes situation for bubble formation. In the post-processing of the pictures it can be seen that the shape of bubbles is squeezed and stretched at high liquid metal velocities. Nevertheless, a complete breakup of bubbles at the beginning could not be detected until the maximum rotation frequency was reached. On the one hand, the bubble size seems to be slightly reduced by small breakups, which are almost not visible with the resolution in neutron radiography for Ar and Ga. On the other hand, the different conditions of pressure and velocity at the orifice can cause a more compact formation of bubbles which are evaluated as smaller bubbles.
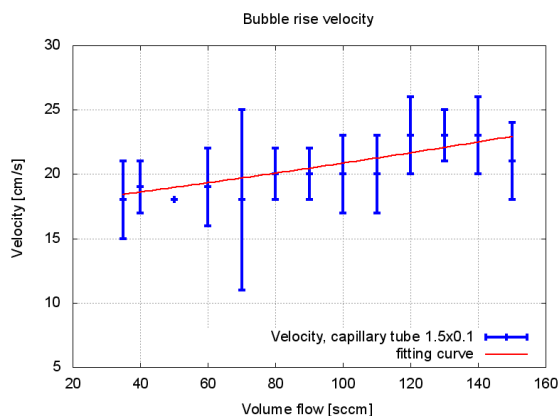
Figure 4. Bubble rise velocity in dependence of volume flow rate. Inlet diameter 0.1 mm. Averaged velocity at each volume flow of ten bubbles.
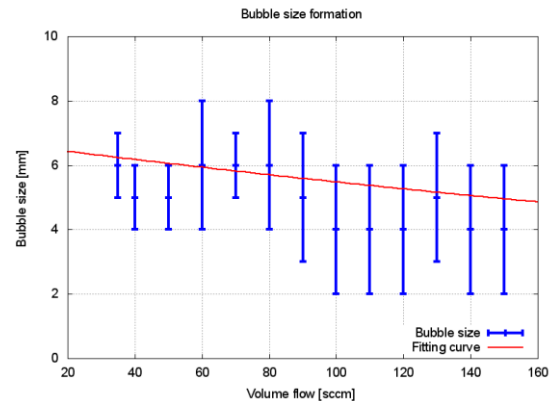
Figure 5. Bubble size in dependence of volume flow rate. Inlet diameter 0.1 mm. Averaged size at each volume flow of ten bubbles.
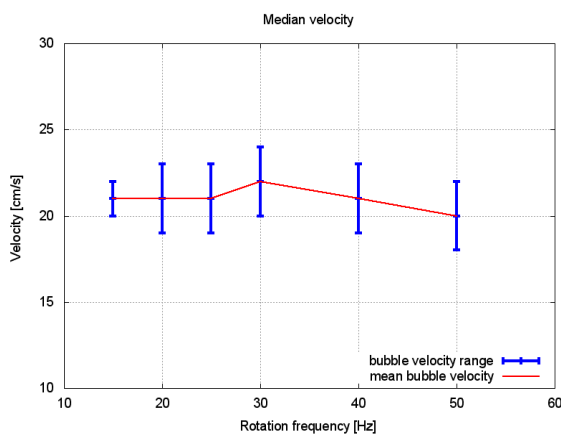
Figure 6. Bubble rise velocity in dependency of rotation frequency of permanent magnets. Inlet diameter 0.1 mm. Flow rate 100 sccm. Averaged velocity at each volume flow of ten bubbles.
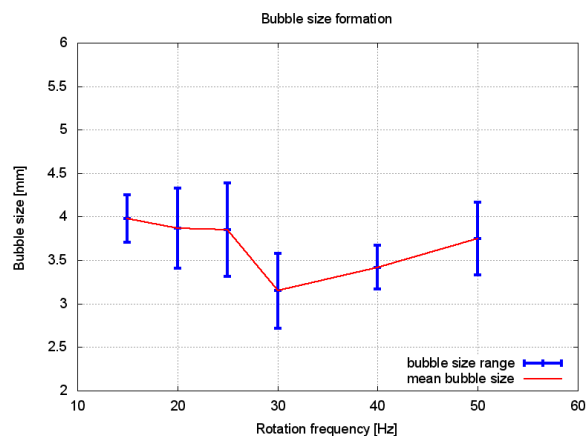
Figure 7. Bubble size formation in dependency of rotation frequency of permanent magnets with error bars representing maximum and minimum size at each flow rate.

5.2. Gallium solidification

After the image post-processing of the raw images the pictures of the ingot growth formation at different time-steps as well as the videos of the crystallization front movement were obtained. Figures 8 shows the evolution of the Ga solidification in constant field and convection, forced by AMF and PMF in time at 20th, 60th and 140th minutes of the process. Here the red colour (darker grey for black/white figure) and its shades correspond to the melt with higher temperature, while the blue colour (light grey) demonstrates the cooled solid phase. According to the equation (1) the colour saturation of different parts of solidified sample corresponds to the different dense of the material.

As it can be seen from the figure 8 (1, a), in the case of constant field two crystallization centres can be recognized – approximately in the middle on the vessel's bottom and on the side of the tank. A development of the first centre was preconditioned by the cooling. Although, an appearance of the second solidification centre is not so clear and can be a consequence of impurity of the glass or a proximity to the melt's free surface and intensive heat transfer from it.
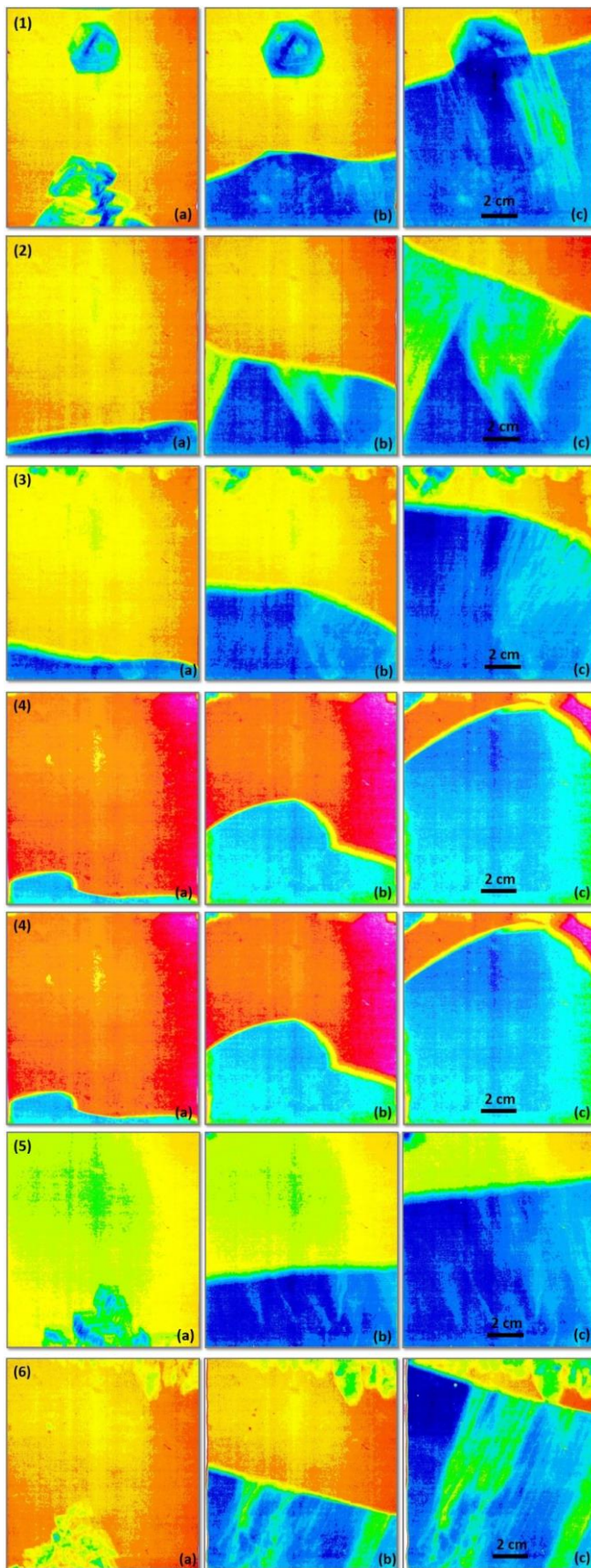
Figure 8. Gallium solidification in conditions of (1) buoyancy driven convection (no rotation of the magnets), (2) forced convection in AMF field (f_{ac} = 23,3 Hz) and in PMF: (3) f_p = 0,025 Hz; (4) f_p = 0,05 Hz; (5) f_p = 0,1 Hz; (6) f_p = 0,25 Hz: (a) 20th minute from the process begin; (b) 60th min; (c) 140th min

On the bottom crystal can be recognized the orthorhombic crystal structure, typical for the α-Gallium as well as several layers of the crystals and their direction of the growth. After 40 minutes from the start of the cooling process the solidification front develops in another way (figure 8 (1-b)). In fact, a growth of initial crystal on the bottom (at 20th min high is 4 cm) took less than 5 min, while for the formation of the main ingot with high 4,2 cm it took one hour. The reason for this phenomenon is an unstable nature of solidifying Ga and corresponding to it an overcooling of the melt.

Due to the intensive melt motion (up to 25 mm/sec, measured with ultrasound Doppler system) the formation of the initial crystal on the bottom for the case of forced convection was prevented. As it shown on the figure 8 (2-6, a-c) a flatter form of the solidification front has appeared at the beginning. For the cases of AMF and PMF with frequencies (figure 8 (2, 4, 6)) the tilt has developed. A reason for the formation of the tilt could be consequence of not homogeneous cooling or the nature of the solidification process, when the already formed solidification front catches the crystals from the flowing liquid. An evidence for the second statement to be true is the behaviour of the tilt growth in the case of mixed melt: regardless to the absence of the influence of the field from the left magnet (see figure 8 (2, 4, 6 - c)) the tilt did not become flat. The flow, produced by the field from the right magnet washes new crystals to the solid front, which grows keeping the tilt angle and the tilt, which once appeared develops with time with increasing of its angle. Triangle forms on the figure 8 (2, a-c) could be the wake from the bulky orthorhombic crystal. Although some of the cases demonstrate denser and more homogeneous structure of the ingot (figure 8 (3-5)), they cannot be compared, due to the individual calibration of the picture contrast for each sample.

As it can be seen for all ingots, formed under the influence of PMF (figure 8 (3-6)) the solidification was starting from the free surface as well as from the cooled bottom. There is a certain reason for such a behaviour: due to the density difference (for solid Ga is lower as for liquid metal) the small crystals, solidified during the stirring were floating to the free surface during the pause between pulses of forcing. The flattest form of a solidification front, corresponding to the most stable process, was obtained for the case of $f_p = 0,1$ Hz (figure 8 (5)). Such a frequency seems to be optimal for PMF application, becoming a compromise between ST and permanently applied AMF.

6. Conclusions

Carried out results show, that neutron radiography can be used to investigate bubble dynamics in liquid metal. Bubble formation, as well as bubble velocity development is highly fluctuating process. For detection of terminal velocity for bubble columns with a height of appr. 1 m, the size of imaging frame is too small. Thus, for reliable data for bubble column reactors a realistic column with a depth of maximum 25 mm has to be manufactured. Together with a sensor at the inlet, which detects bubble formation the camera can be adjusted to the surface and terminal velocity can be calculated more reliable. In order to study bubble formation and velocity distribution of the liquid melt, particle tracers and PIV can be utilized. Regarding separation of bubbles, more powerful magnets and adjusted gears for higher rotation speed will lead to higher induced shear stresses and mixing of bubbles.

Thermal neutron radiography is suited for visualization of solidification process in different conditions. Nonetheless the range of materials, which can be employed to the experiment is limited, this technique provides essential information about the complex process of formation of solidifying material. Such low-temperature metals as Gallium, Caesium, and Tin provide high-contrast neutron images. At the same time melts of these metals could be stirred by application of EM field. Information about the mechanisms of interaction between the forced melt flows and a solidification front and the form of solid/liquid interface, demonstrating thermal conditions, can be obtained by means of neutron radiography. Another advantage of this investigation method in comparison to the analogies is possibility to work with relatively thick samples, so an influence of a three – dimensional turbulence phenomena could be analysed. The results of Ga solidification in conditions of buoyancy driven and forced by alternating magnetic field convection have shown that the process of solid front formation can be influenced by the intensive melt flow. More flat form and absence of the initial bulky crystals can be stated for the case of forced convection.

References
[1]   Tarapore E D and Evans J W 1977 *Met. Mater. Trans.* B **7B** 345–351
[2]   Moore D J and Hunt J C R 1983 *Progress in Astronautics & Aeronautics* **84** 359–373
[3]   Umbrashko A 2010 *Heat and Mass Transfer in Electromagnetically Driven Recirculated Turbulent Flows* PhD thesis (Physics) (Riga: Latvian University) p 108
[4]   Kirpo M 2008 *Modeling of Turbulence Properties and Particle Transport in Recirculated Flows* PhD thesis (Physics) (Riga: Latvian University) p 188
[5]   Koster J N 1997 *JOM* **49** 31–35
[6]   Boden S, Eckert S, Willers B and Gerbeth G 2008 *Metall. Mater. Trans.* A **39** 613–62
[7]   Shevchenko N, Boden S, Eckert S, Borin D, Heinze M and Odenbach S 2013 *Eur. Phys. J. Special Topics* **220** 63–77
[8]   Jasti J K and Fogler H S 1992 *AIChE Lournal* **38** 481–488
[9]   Kim B 2002 *Development of Macrosegregation During Solidification of Binary Metal Alloys* PhD thesis (Mech. Eng.) (USA: Pennsylvania State Univ.) p 255
[10]   Wondrak T, Eckert S, Gerbeth G, Stefani F, Timmel K, Peyton AJ, Terzija N and Yin W 2014 *Steel Research Int.* **85** 1266–73
[11]   Saito Y, Mishima K, Tibita Y, Suzuki T and Matsubayashi M 2004 *Appl Radiation and Isotopes* **61** 983–691
[12]   Sarma M, Scepanskis M, Jakovics A, Thomsen K, Nikoluskins R, Vontobel P, Beinerts T, Bojarevics A and Platacis E 2015 *Physics Procedia* **69** 457–463
[13]   Fehling T, Steinberg T and Baake E 2017 *Int. J. of Appl. Electromagnetics and Mechanics* **53** S1, S111–S120
[14]   Drew D A 1983 *Ann. Review Fluid Mech.* **15** 261–291
[15]   Yang Z, Seo P K and Kang C G 2005 *J. Mater. Sci. Technol* **21** 219–225
[16]   Vives C 1986 *J. Cryst. Growth* **76** 170–184
[17]   Buschow K H J 2001 Encyclopedia of Materials: Science and Technology (Amsterdam: Elsevier Science Ltd.) 4733–39
[18]   Eckert S, Nikrityuk P A, Räbiger D, Eckert K and Gerbeth G 2007 *Metall. Mater. Trans.* B **38** 977–988
[19]   Willers B, Eckert S, Nikrityk P A, Räbiger D, Dong J, Eckert K and Gerbeth G 2008 *Metall. Mater. Trans.* B **39B** 304–316
[20]   Wang X, Fautrelle Y, Etay J and Moreau R 2009 *Metall. and Mater. Trans.* **40B** 82–90
[21]   Sears V F 1992 *Neutron News* **3** 26–37
[22]   Kolesnichenko A F, Podoltsev A D and Kucheryavaya I N 1994 *ISIJ Int* **34** 715–721
[23]   Fehling T, Steinberg T and Baake E 2017 *Proceedings of XVIII International UIE Congress*: *Electrotechnologies for Material Processing* 416-421